

# DIC2CAE: Calculating the stress intensity factors ( $K_{I-III}$ ) from 2D and stereo displacement fields

Abdalrhaman Koko <sup>a,b\*</sup>

<sup>a</sup> National Physical Laboratory, Hampton Road, Teddington TW11 0LW, United Kingdom

<sup>b</sup> Department of Materials, University of Oxford, Oxford OX1 3PH, United Kingdom

## Abstract

Integrating experimental data into simulations is crucial for predicting material behaviour, especially in fracture mechanics. Digital Image Correlation (DIC) provides precise displacement measurements, essential for evaluating strain energy release rates and stress intensity factors (SIF) around cracks. Translating DIC data into CAE software like ABAQUS has been challenging. DIC2CAE, a MATLAB-based tool, automates this conversion, enabling accurate simulations. It uses the  $J$ -integral method to calculate SIFs and handles complex scenarios without needing specimen geometry or applied loads. DIC2CAE enhances fracture mechanics simulations' reliability, accelerating materials research and development.

**Keywords:**  $J$ -integral; Digital image correlation; Finite element analysis; Stress-intensity factor.

---

\* Corresponding author email address: [abdo.koko@npl.co.uk](mailto:abdo.koko@npl.co.uk)

## Code metadata

---

Current code version	V1.0.1
Permanent link to code	-
Code Ocean compute capsule	N/A
Legal Code License	MIT License
Code versioning system used	git
Software code languages	MATLAB
Compilation requirements	MATLAB R2021a or later and ABAQUS
Link to developer documentation	<a href="https://github.com/Shi2oon/DIC2CAE">https://github.com/Shi2oon/DIC2CAE</a>
Support email for questions	<a href="mailto:abdo.koko@npl.co.uk">abdo.koko@npl.co.uk</a>

---

# 1. Motivation and significance

Fracture mechanics focuses on understanding and predicting the propagation of cracks, which involves quantifying the conditions required for crack growth. A key concept is the strain energy release rate, representing the potential energy available to extend a crack. In linear elastic materials or under small-scale yielding (SSY) conditions, the strain energy release rate can be linked to the stress intensity factor (SIF), a descriptor of the stress field around a crack. Even when crack tip plasticity invalidates SSY, the strain energy release rate remains a useful metric [1–3].

DIC allows precise full-field displacement measurement by tracking patterns between images, including parasitic fields induced due to sample misalignment [4]. In addition, techniques such as field fitting, and the  $J$ -integral are used to calculate the SIF and strain energy release rate from DIC data. The  $J$ -integral, which calculates the energy release rate from the strain field, is particularly robust against uncertainties near the crack tip. This method is widely implemented in finite element software and can integrate experimental displacement data, ensuring accurate analysis of the crack field, even under complex conditions. Compared to using the Williams' series least square fitting method, it is less sensitive to knowledge of the exact position of the crack tip [5–7].

The significance of DIC2CAE lies in its ability to bridge this gap. By automating the process of converting DIC data into CAE-compatible formats, the code enables researchers and engineers to incorporate real-world experimental data more easily into their simulations. This integration enhances the accuracy and reliability of simulations, leading to better predictions of material performance and failure. Moreover, DIC2CAE facilitates a more efficient workflow, reducing the time and effort required to prepare experimental data for simulation. This efficiency allows for more iterative testing and validation, ultimately accelerating the development of new materials and improving the understanding of existing ones. In essence, DIC2CAE empowers users to leverage the full potential of DIC data in their computational models, driving advancements in materials science and engineering.

## 2. Software description

The software, implemented in MATLAB, interacts with ABAQUS to calculate the stress intensity factor (SIF) directly from the displacement field measured digital image correlation (DIC), including stereo-DIC (Figure 1a and b), where two cameras are used to measure not only the in-plane displacement fields but also the out-of-plane displacement field.

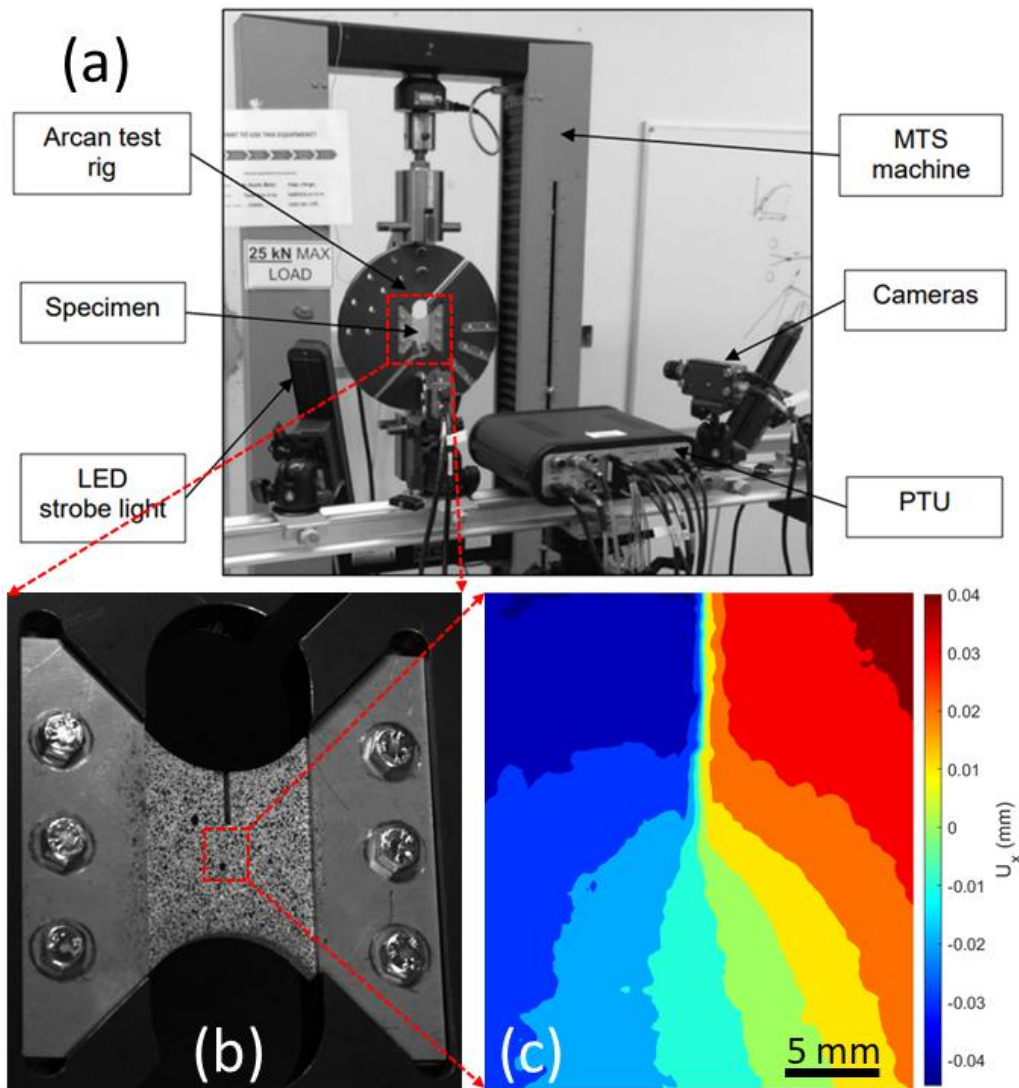


Figure 1: (a) An Arcan test fixture with a speckled butterfly sample and stereo digital imaging system. (b) Image of the field of view of the loaded speckled butterfly sample. (c) The  $U_x$  displacement field that is obtained by digital image correlation of the speckled field of view.

The main function requires the user to input the location of the DIC data and the material's mechanical properties which can be an isotropic or anisotropic elastic material, or a plastic material that follows Ramberg–Osgood relationship. Afterwards, the user specifies the crack tip location and any noisy areas around it that should be masked. The program uses a finite

element method (FEM) to calculate the  $J$ -integral from the displacement data provided by DIC, as shown in Figure 1c. A Python script, which is automatically written using the MATLAB code, handles the creation of a finite element model in ABAQUS that aligns with the DIC data, ensuring both share the same coordinate system. Matching the finite element mesh with the DIC grid avoids interpolation when applying the displacement field.

The calculations use a rectangular grid with four nodes per plane stress element (ABAQUS' CPS4). Node displacements are imposed as boundary conditions, except in the noisy region near the crack. This is because, despite DIC precision, it faces challenges in capturing displacements near discontinuities like cracks. Thus, finite element-based interpolations are used to enhance DIC accuracy and data reliability, offering better insights into crack behaviour and improving fracture mechanics analysis.

The ABAQUS software then applies material laws and selects between plane stress and plane strain elements. The  $J$ -integral is calculated using a domain integral (EDI) method with a Virtual Crack Extension technique [8]. This method calculates the potential elastic strain energy release rate and separates mode I and II stress intensity factors. The EDI method starts at the crack tip and propagates in the direction of a virtual extension, with a smooth function ( $q$ ) varying from unity at the tip to zero at the outer domain. The  $q$ -vector is normal to the crack front, aligning with the crack path. Multiple contours are used in the  $J$ -integral calculation to ensure contour independence, determining the potential release of elastic strain energy from crack propagation based on the displacement field.

For the stereo-DIC field, which contains the out-of-plane displacement field ( $U_z$ ), mode III is calculated by injecting the field as  $U_x$  displacement. The antisymmetric (pseudo) shear stress intensity factor ( $K_{II}^{\text{pseudo}}$ ) is calculated by ABAQUS, and the pseudo-in-plane shear mode II SIF is then corrected to an out-of-plane mode III SIF as described in equation (1), where  $E$  is Young modulus and  $G$  is the shear modulus.

$$K_{III} = \frac{2G}{E} K_{II}^{\text{pseudo}} \quad (1)$$

It should be highlighted that the orientation of the in-plane shear (II) and out-of-plane shear (III) components is not significant in this scenario, as it is determined by the nodal

configuration at the crack tip and lacks physical relevance. In contrast, the sign of mode I is critical, as it indicates whether tensile or compressive forces are acting at the slip band tip. Additionally, the symmetric out-of-plane component of mode I remains unaffected by the orientation of the mode III stress intensity factor. Moreover, although the current analysis focuses on the displacement fields captured using DIC, there are methods that can be used to integrate strain fields to obtain the displacement fields [9,10], which can also be analysed through this code.

## 2.1. Software architecture

The system is organised into several key modules, each dedicated to handling specific tasks within the analysis pipeline. This modular framework enhances flexibility, allowing users to adapt the software to various complex scenarios, including the detailed study of crack propagation and material behaviour under stress. Examples of how to validate the code are provided in "InputDesk\_Validate", which will be discussed further in section 3, and an example of how to use the code with typical DIC data is shown in "InputDesk\_DIC".

## 2.2. Software functionality

The "InputDesk\_DIC" function provides an input script for the function *DIC2CAE*, which is designed to process DIC data to analyse the crack tip and calculate fracture mechanics parameters such as the *J*-integral and stress intensity factors ( $K_I$ ,  $K_{II}$ , and  $K_{III}$ ).

The script begins by clearing the workspace, closing all figures, and adding a specific path that contains necessary functions. It then defines the location of the DIC data file (here is "2D\_DIC.dat") and sets up the folder where the results will be saved. The script's main part involves configuring the DIC data analysis parameters. These parameters include the physical units (meters, millimetres, or micrometres) and the size of the domain. The script specifies whether the analysis will handle plane stress or plane strain conditions.

Next, the material properties are defined. In this case, the material is defined as Ferrite, with a Poisson's ratio of 0.3 and a Young's modulus of 210 GPa. The material type is set to 'E', indicating that it is elastic. The script has additional placeholders for other types of material behaviour, such as elastoplastic or anisotropic materials, though these are not used in this particular setup.

The "DIC2CAE" function in the repository is designed to bridge the gap between digital image correlation (DIC) data and Computer-Aided Engineering (CAE) software. This function is crucial in transforming experimental data into a format that can be utilised for simulations and analyses in CAE tools like ABAQUS. This includes calculating the effective Young's modulus, shear modulus and Poisson's ratio for anisotropic materials through the "effectiveE\_v" function based on ref. [11] and only valid for cubic materials. This information will be needed later to calculate the SIFs from the strain energy release rate.

The "Locate\_Crack" function—within the DIC2CA function—is designed to identify the crack with the option of rotating the displacement field and cropping the field of view. After preprocessing, the function moves on to the crack detection step, where the user selects the crack tip and end and then selects the noise region around the crack that needs to be masked to allow for finite-element-based interpolation, as shown in Figure 2. This information about the crack will later be used to build the finite element model inside ABAQUS.

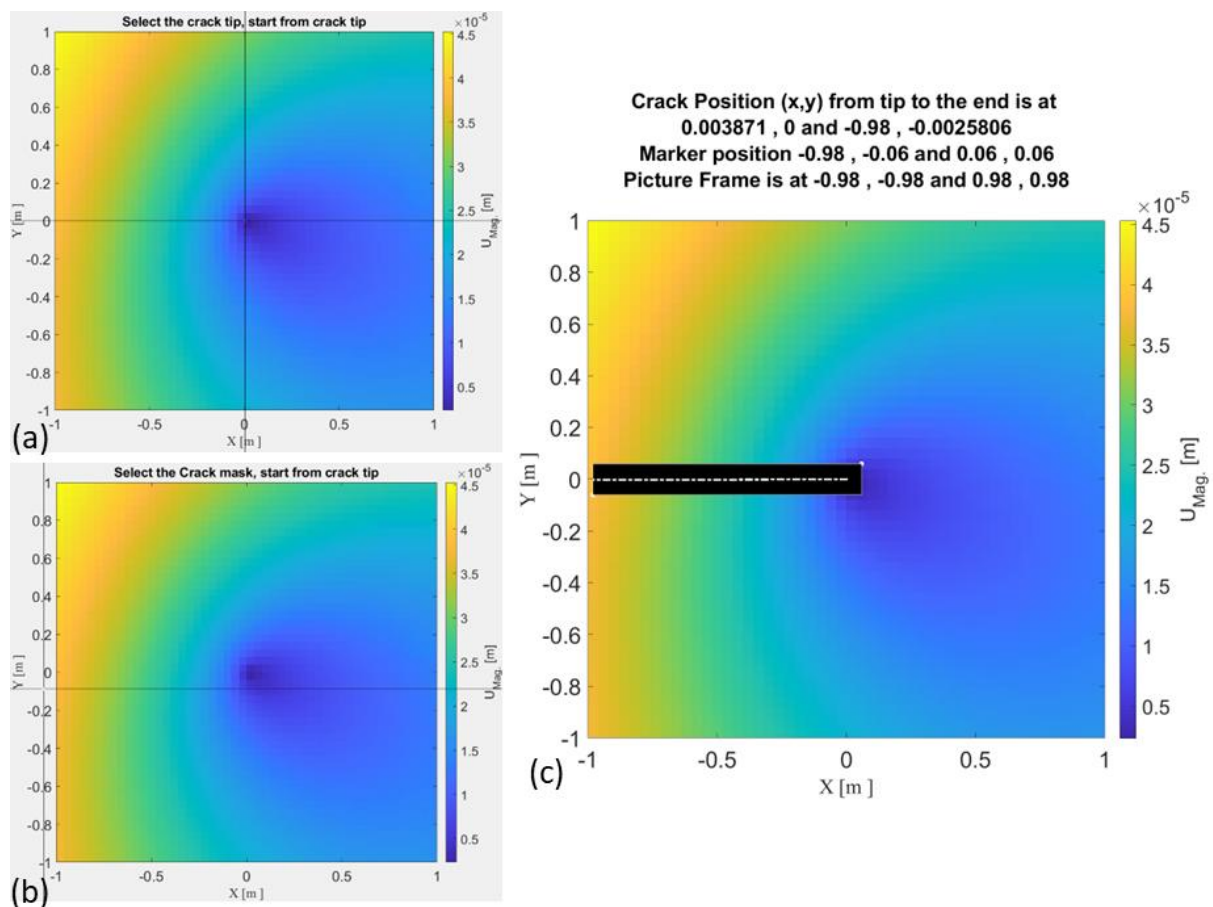


Figure 2: When you run the script after it loads the displacement field, it plots the displacement magnitude (UMag) to allow the user to (a) select the crack starting from the crack tip, and (b) select

the area to mask where the crack is producing noisy data. (c) The user selected crack (dotted white lines) and the masked area (black square) projected on the  $U_{Mag}$ .

The "PrintRunCode" function generates and manages the code necessary to run simulations based on the processed DIC data. The function begins by setting up the environment for the simulation, which involves defining the parameters and variables that will be used throughout the simulation process. These parameters might include material properties, boundary conditions, and other essential simulation settings. The crack direction (q-vector) is assumed to lie on the horizontal axis.

One of the primary sub-functions within "PrintRunCode" is the code generation step. This sub-function creates the actual Python code, and the CAE software will execute automatically. It takes the processed DIC data and translates it into a format that the CAE software can understand. This involves generating input files or scripts that set up the simulation, defining the material's properties, including the field and crack geometry, mesh, and boundary conditions, and executing the analysis. In addition, accurate FEM analysis requires high-quality computational meshes that can capture the intricate details of stress and strain distributions within the material. The software includes robust tools for generating these meshes and re-meshing regions during the simulation. The "RemeshCrackedRegion" sub-function is particularly important, as it allows for the adaptive refinement of the mesh around crack tips or other areas of interest.

The "PrintRunCode" function also includes a sub-function for managing the simulation output. This involves defining how the simulation results will be stored and accessed. The output management sub-function ensures that the simulation results are saved in a format that can be easily analysed and interpreted, as shown in Figure 3. This includes generating output files or setting up data structures to store the simulation results.



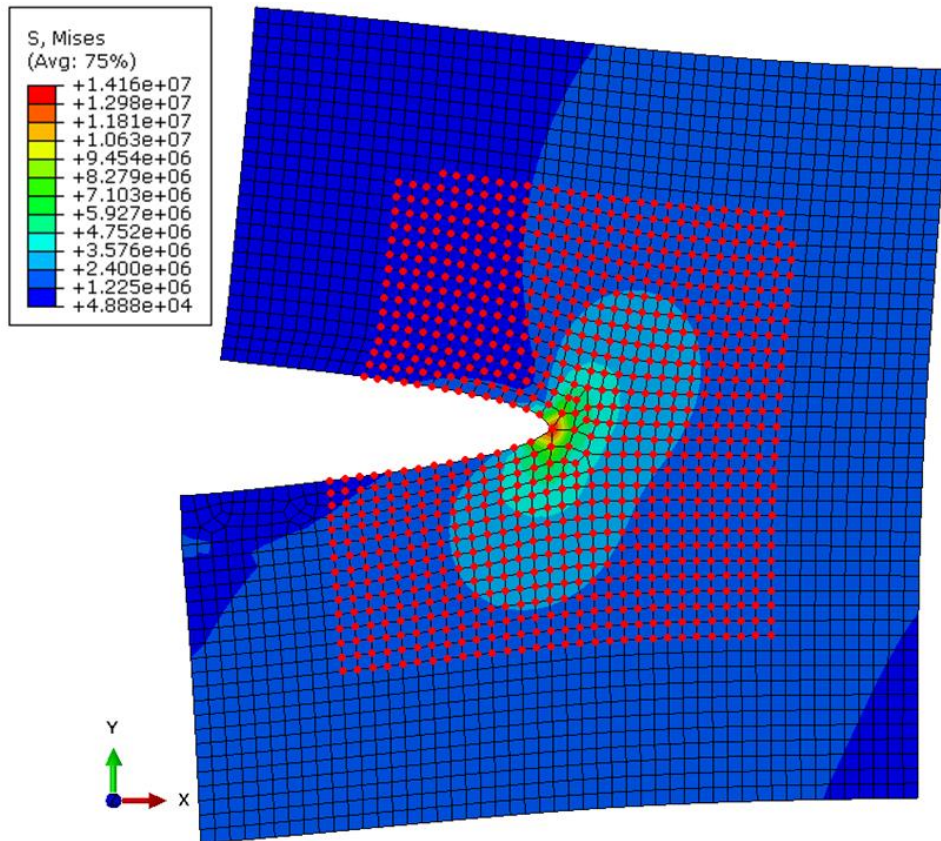


Figure 3: Deformed configuration of the von Mises stress around the crack calculated from the DIC displacement field. The red nodes donate the domain to be integrated for the  $J$ -integral calculation. The domain starts from the crack tip and expands incrementally to engulf the entire field of view.

Finally, the "PrintRunCode" function includes a sub-function for logging and documentation. This sub-function keeps track of the simulation process, including any errors or warnings during the code generation and execution steps. The logging and documentation sub-function ensures that there is a clear record of the simulation process, which can be useful for debugging and future reference.

After the CAE is done, the "PlotKorJ" function is designed for the CAE output data extraction, including the  $J$ -integral and SIFs, through the "readDATABAQUS" sub-function, to prepare it for visualisation. This sub-function opens the ABAQUS output files and reads the data contained within them. It handles various file formats that ABAQUS produces, such as ODB (output database) files or text-based output files. The file reading step is crucial because it extracts the raw data needed for subsequent analyses. After reading the files, the function moves to the data parsing step. This sub-function processes the raw data to extract meaningful information. It parses the data to identify relevant parameters, such as  $J$ -integral

and SIFs. The parsing step ensures that the data is organised and structured to make it suitable for further analysis and visualisation. It also asks the user to select the number of contours to consider, as convergence might fail when the domain expands to the peripheral fields of other stress raisers. As discussed by [12,13], their contribution to the gradient field makes the vector field non-conservative unless fully engulfed by the integration domain, so the integral at the far field will not be path-independent. See the video in the supplementary material for the visualisation of convergence with the integration domain expansion.

Afterwards, the "Adjust4Direction" function is designed to adjust the directionality of the q-vector for  $J$ -integral calculation from the ABAQUS output, which can indicate the possible direction for the crack to propagate. The "Adjust4Direction" function can also handle user inputs and repeat the computational process but the new crack direction (or q-vector).

Finally, the  $J$ -integral and SIFs values per contour are organised, and the area where the integration convergence (shaded pink in Figure 5) is used to calculate the mean  $J$ -integral and SIFs values and variance, before being visualised using the "plotJKIII" function, as shown in Figure 5.

### 3. Illustrative examples and error analysis

The stress concentrations of a crack were considered to assess the errors in the  $J$ -integral analysis and decomposition of modes. This was generating using the "Calibration\_2DKII" function. A synthetic displacement field for a mixed-mode crack in an infinite body was created that has a mode I stress intensity factor ( $K_I$ ) of 3 MPa m<sup>0.5</sup>, mode II ( $K_{II}$ ) of 1 MPa m<sup>0.5</sup>, and mode III ( $K_{III}$ ) of 5 MPa m<sup>0.5</sup>, using an analytical solution [14] and assuming plane strain conditions (eq. 3—1). The elastic modulus ( $E$ ) and Poisson's ratio ( $\nu$ ) were 210 GPa and 0.3, respectively. The data are presented in the field of view of 1 x 1 m<sup>2</sup>, with 0.02 x 0.02 m<sup>2</sup> square elements, and the crack tip was placed at the centre (0,0).

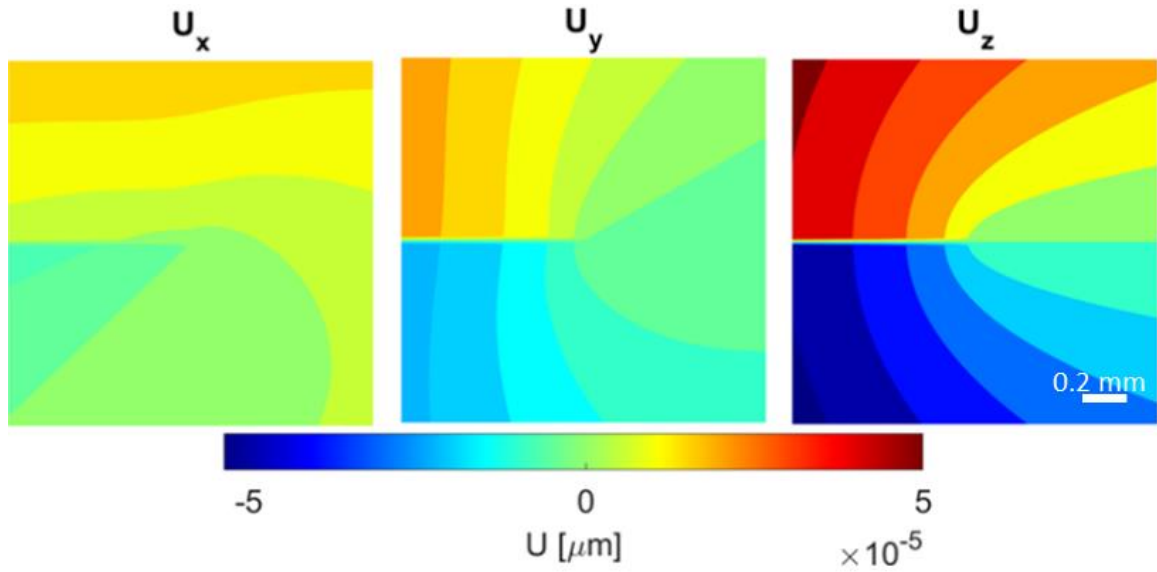


Figure 4: Synthetic  $U_x$ ,  $U_y$ , and  $U_z$  displacement field components with the crack tip being at the centre.

$$\begin{Bmatrix} U_x \\ U_y \\ U_z \end{Bmatrix} = \frac{1}{\mu} \sqrt{\frac{r}{2\pi}} \begin{bmatrix} \cos \frac{\theta}{2} \left( 1 - 2\nu + \sin^2 \frac{\theta}{2} \right) & \sin \frac{\theta}{2} \left( 2 - 2\nu + \cos^2 \frac{\theta}{2} \right) & 0 \\ \sin \frac{\theta}{2} \left( 2 - 2\nu - \cos^2 \frac{\theta}{2} \right) & \cos \frac{\theta}{2} \left( -1 + 2\nu + \sin^2 \frac{\theta}{2} \right) & 0 \\ 0 & 0 & 2 \sin \frac{\theta}{2} \end{bmatrix} \begin{Bmatrix} K_I \\ K_{II} \\ K_{III} \end{Bmatrix} \quad 3-1$$

$$\text{Shear modulus } (\mu) = \frac{E'}{2(1 + \nu)}, \quad E' = \frac{E}{1 - \nu^2}$$

Synthetic  $U_x$ ,  $U_y$ , and  $U_z$  displacement fields around the stationary mixed mode crack were used to calculate in-plane symmetrical mode I SIF, in-plane asymmetrical mode II SIF, and out-of-plane asymmetrical mode III SIF (Figure 4). The EDI method implemented in ABAQUS® was used on the decomposed fields. Stabilised convergence is achieved as the domain expands, with the calculated  $J$ -integral and decomposed stress intensity factors matching the values used as inputs to create the field, except for small contours where highly localised fields close to the crack tip influenced initial convergence (Figure 5).

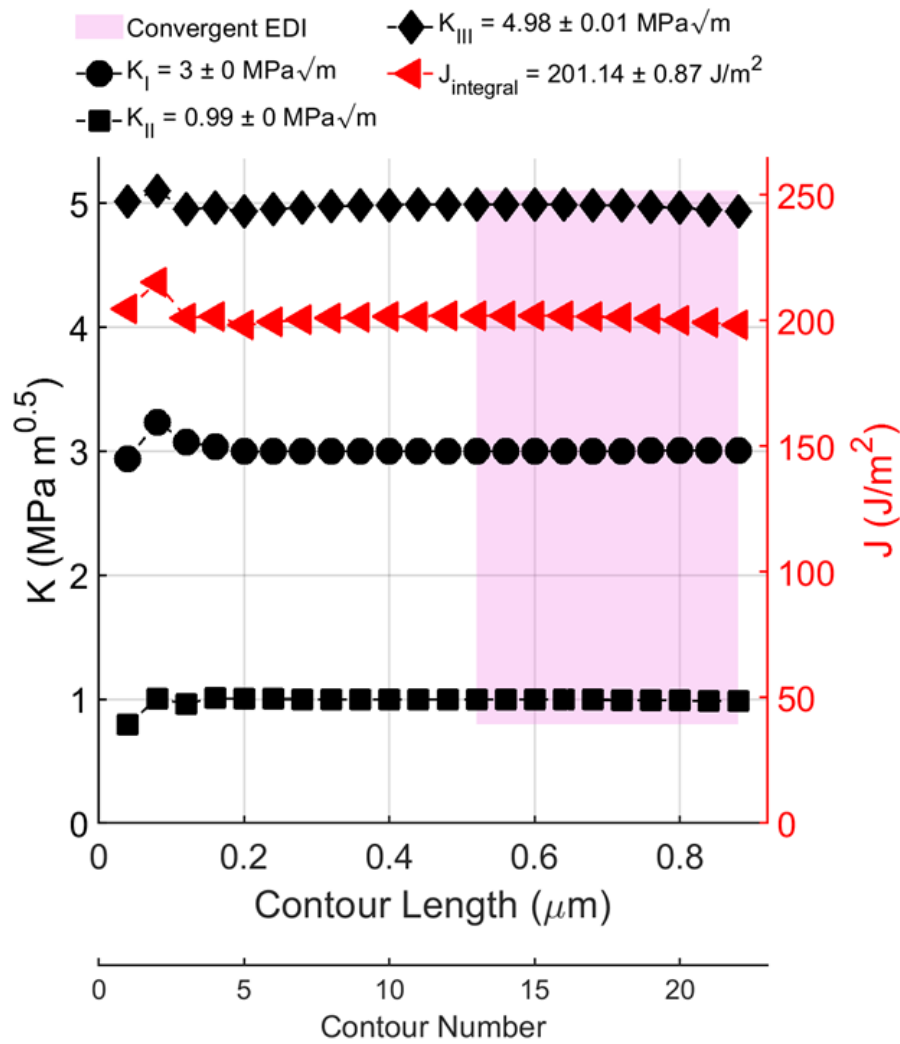


Figure 5:  $J$ -integral and decomposed loading modes as a function of contour distance from the crack tip. The represented values are calculated from the highlighted pink area.

The key sources of errors were assessed. First, a noise signal was randomly distributed to each displacement component. The magnitude of the signal increased from 0.0001% to 1% of the field mean magnitude, and the effect on the  $J$ -integral and SIFs were then studied. As shown in Figure 6, the EDI convergence decreased with increasing noise; hence, the uncertainty error in the value increased. The mean  $K_I$  and  $J$ -integral values decreased, and the  $K_{II}$  values increased, although  $K_{III}$  was not adversely affected by the noise.

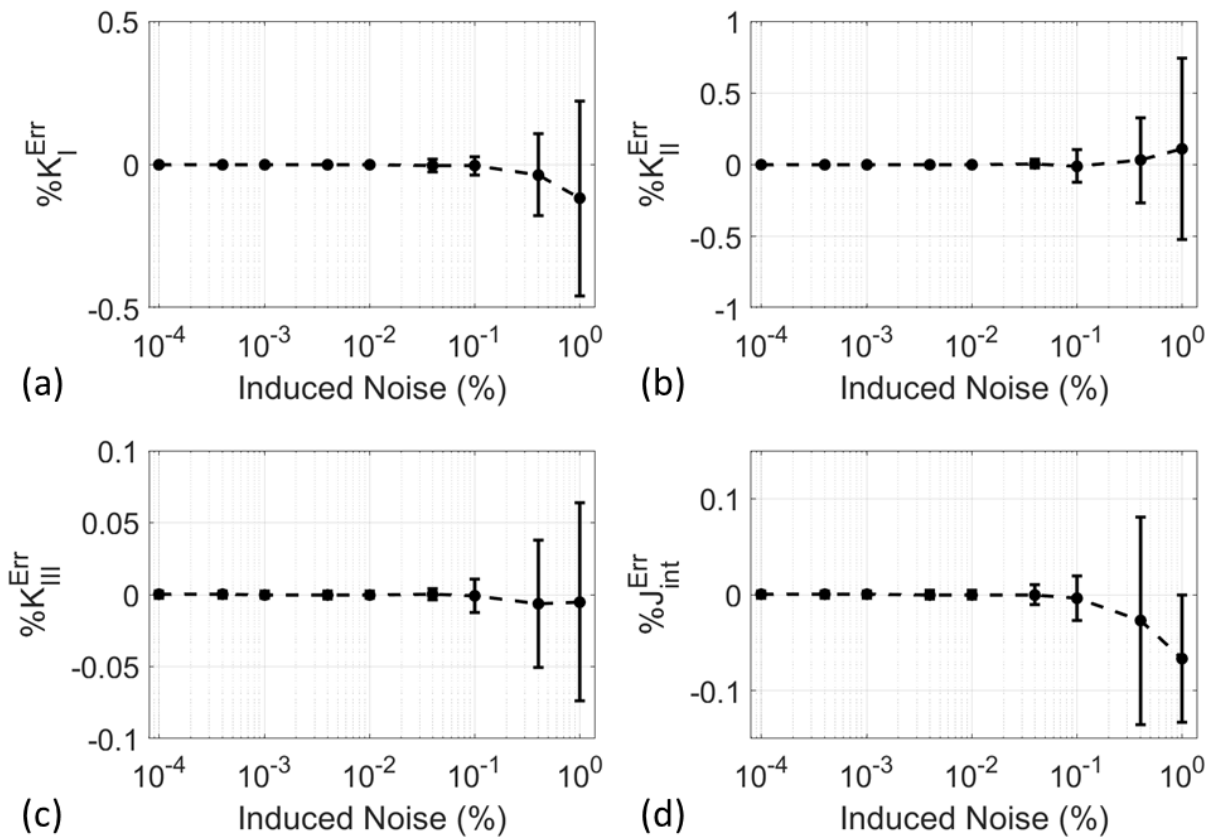


Figure 6: (a)  $K_I$ , (b)  $K_{II}$ , (c)  $K_{III}$ , and (d)  $J$  normalised error analysis with induced random.

Second, the sensitivity of the analysis to crack tip location was assessed relative to the accurate crack tip position, which was at the origin (0,0) coordinate. The (normalised) error in accurately locating the crack increases if the location was assumed to be ahead, relative to assuming the same distance behind the crack (Figure 7). In  $K_I$  and  $K_{II}$  analysis, the values are less affected by inaccuracy along the X-axis. However, for mode I, positional inaccuracies in the Y-axis increase the value if the crack was inaccurately located under its correct position and vice versa compared to mode II, which varies symmetrically as the tip deviates along the Y-axis. In  $K_{III}$  analysis, deviation from the tip is more complex but generally increases the value of  $K_{III}$ . The induced errors in each decomposed field combine and form the complex error (Figure 7a).

The overall trend of the SIFs is that uncertainties in the Y-axis position relative to the true position of the crack have more adverse effects than the X-axis. The sensitivity to the crack position does not affect the EDI convergence for SIF calculation (Figure 7e) but mainly affects the value. However, it seems to affect both the convergence and the value for the  $J$ -integral.

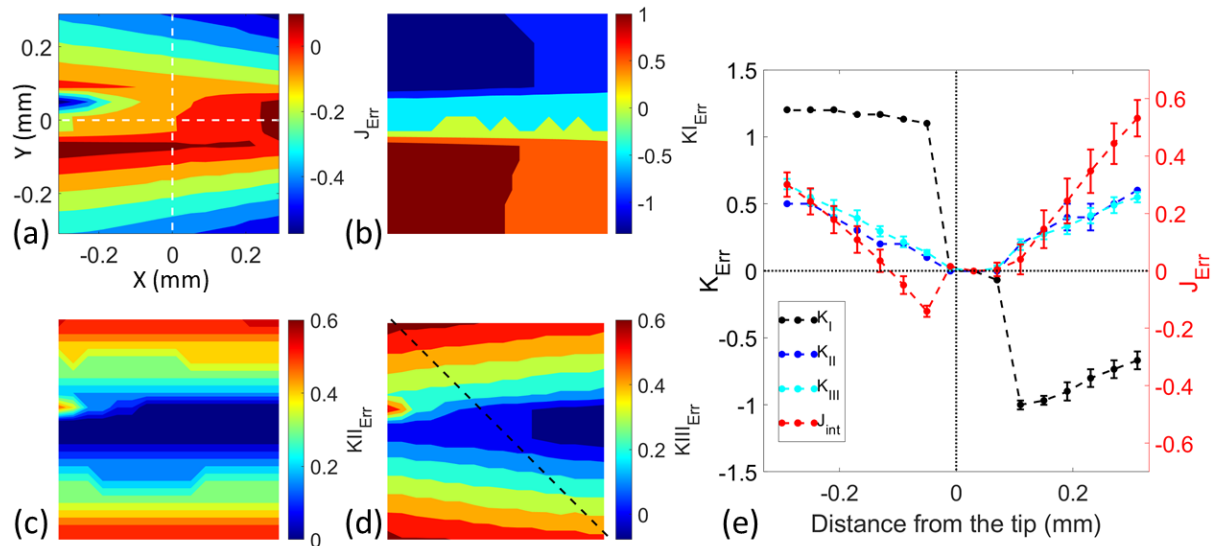


Figure 7: (a)  $J$ , (b)  $K_I$ , (c)  $K_{II}$  and (d)  $K_{III}$  normalised error analysis of the sensitivity to crack tip position originally at (0,0) highlighted by dashed white lines in (a). (e) The diagonal line profile (highlighted by the dashed black line in (d)) of the  $J$ -integral and decomposed SIFs.

Overall, the proposed method was validated using the synthetic displacement field of a crack under mixed-mode loading, including the effect of noise and uncertainty of crack tip on the  $J$ -integral and SIFs values which affect the EDI convergence and the  $J$ -integral and SIFs values, especially on the Y-axis (i.e., perpendicular to the crack direction).

## 4. Impact

Direct measurements of the strain energy release rate and SIF are necessary to quantify crack fields accurately. Traditionally, these are calculated using known boundary conditions, specimen geometry, and applied loads. However, challenges arise when residual stresses, crack closure, or uncertain boundary conditions (due to manufacturing defects or experimental inaccuracies) interfere with these calculations. Consequently, methods for direct measurement of the crack field, such as digital image correlation (DIC), have gained interest [15–18].

The DIC2CAE code is motivated by the need to seamlessly integrate experimental data from DIC into Computer-Aided Engineering (CAE) simulations. DIC is a powerful technique for measuring full-field displacements and strains on material surfaces, providing detailed insights into material behaviour under various loading conditions. However, translating this rich experimental data into formats usable by CAE software like ABAQUS has traditionally

been challenging. This is because calculating the SIF using finite element analysis (FEA) through tools like ABAQUS offers significant advantages over traditional analytical methods. While analytical solutions are often limited to simple geometries and loading conditions, FEA in ABAQUS can accommodate complex geometries, non-standard crack shapes, and varied load scenarios, making it highly versatile for real-world applications. Additionally, ABAQUS allows for the simulation of non-linear material behaviour, including plasticity, which is crucial for accurately calculating SIF in materials where plastic deformation occurs near the crack tip. This capability contrasts with analytical methods, which generally assume linear elasticity.

Furthermore, FEA enables localised mesh refinement around the crack tip, capturing the steep stress gradients more precisely than analytical approaches. Integrating ABAQUS with custom scripts also enhances analysis flexibility, which is impossible with traditional methods. Importantly, as mentioned earlier, the domain integral method used in ABAQUS, such as the  $J$ -integral, ensures contour-independent SIF calculations, adding robustness and reliability to the results. These factors make FEA in ABAQUS a superior choice for SIF calculation compared to conventional analytical techniques [8,19].

## 5. Conclusion

The DIC2CAE tool provides a robust and efficient solution for integrating Digital Image Correlation (DIC) data into Computer-Aided Engineering (CAE) simulations, particularly in the context of fracture mechanics. By automating the process of converting DIC data into ABAQUS-compatible formats, the software enhances the accuracy of stress intensity factor (SIF) calculations and  $J$ -integral analyses, even under complex conditions such as mixed-mode fractures and crack tip plasticity. The tool's ability to directly incorporate real-world experimental data into finite element models reduce the need of using analytical solutions, and improves the reliability of simulations and accelerates the research and development cycle in materials science. The validation examples and error analyses demonstrate the software's effectiveness in handling noise and positional inaccuracies, emphasising its utility in academic and industrial research.

## Acknowledgements

The authors thank Dr Louise Crocker and Dr Dalia Y. Ali for proofreading the article and the National Measurement System (NMS) programme of the UK government's Department for Science, Innovation and Technology (DSIT) for financial support.

## Conflict of interest statement

The authors declare that they have no known competing financial interests or personal relationships that could have appeared to influence the work reported in this paper.



## References

- [1] Rice JR. Some remarks on elastic crack-tip stress fields. *Int J Solids Struct* 1972;8:751–8. [https://doi.org/10.1016/0020-7683\(72\)90040-6](https://doi.org/10.1016/0020-7683(72)90040-6).
- [2] Rice JR. Limitations to the small scale yielding approximation for crack tip plasticity. *J Mech Phys Solids* 1974;22:17–26. [https://doi.org/10.1016/0022-5096\(74\)90010-6](https://doi.org/10.1016/0022-5096(74)90010-6).
- [3] Rice JR. A Path Independent Integral and the Approximate Analysis of Strain Concentration by Notches and Cracks. *J Appl Mech* 1968;35:379–86. <https://doi.org/10.1115/1.3601206>.
- [4] A T Fry; M Lodeiro; A Koko; F Booth-Downs; L E Crocker. Effect of specimen misalignment in fatigue testing of small-scale test pieces. Teddington: 2023.
- [5] Moutou Pitti R, Badulescu C, Grédiac M. Characterization of a cracked specimen with full-field measurements: direct determination of the crack tip and energy release rate calculation. *Int J Fract* 2014;187:109–21. <https://doi.org/10.1007/s10704-013-9921-5>.
- [6] Molteno MR, Becker TH. Mode I-III Decomposition of the J -integral from DIC Displacement Data. *Strain* 2015;51:492–503. <https://doi.org/10.1111/str.12166>.
- [7] BECKER TH, MOSTAFAVI M, TAIT RB, MARROW TJ. An approach to calculate the J -integral by digital image correlation displacement field measurement. *Fatigue Fract Eng Mater Struct* 2012;35:971–84. <https://doi.org/10.1111/j.1460-2695.2012.01685.x>.
- [8] Courtin S, Gardin C, Bézine G, Ben Hadj Hamouda H. Advantages of the J-integral approach for calculating stress intensity factors when using the commercial finite element software ABAQUS. *Eng Fract Mech* 2005;72:2174–85. <https://doi.org/10.1016/j.engfracmech.2005.02.003>.
- [9] Barhli SM, Saucedo-Mora L, Simpson C, Becker T, Mostafavi M, Withers PJ, et al. Obtaining the J-integral by diffraction-based crack-field strain mapping. *Procedia Structural Integrity* 2016;2:2519–26. <https://doi.org/10.1016/j.prostr.2016.06.315>.

- [10] Koko A, Marrow J, Elmukashfi E. A Computational Method for the Determination of the Elastic Displacement Field using Measured Elastic Deformation Field. To Appear 2021;5. <https://doi.org/https://doi.org/10.48550/arXiv.2107.10330>.
- [11] Luan X, Qin H, Liu F, Dai Z, Yi Y, Li Q. The Mechanical Properties and Elastic Anisotropies of Cubic Ni<sub>3</sub>Al from First Principles Calculations. *Crystals (Basel)* 2018;8. <https://doi.org/10.3390/cryst8080307>.
- [12] Shi MX, Huang Y, Gao H. The J-integral and geometrically necessary dislocations in nonuniform plastic deformation. *Int J Plast* 2004;20:1739–62. <https://doi.org/10.1016/J.IJPLAS.2003.11.013>.
- [13] Kuang JH, Chen YC. The values of J-integral within the plastic zone. *Eng Fract Mech* 1996;55:869–81. [https://doi.org/https://doi.org/10.1016/S0013-7944\(96\)00077-X](https://doi.org/https://doi.org/10.1016/S0013-7944(96)00077-X).
- [14] Anderson TL. *Elastic-Plastic Fracture Mechanics. Fracture Mechanics - Fundamentals and Applications*. 4th ed., CRC Press; 2017, p. 688.
- [15] Becker TH. Extracting fracture properties from digital image and volume correlation displacement data: A review. *Strain* 2023. <https://doi.org/10.1111/str.12469>.
- [16] Koko A, Earp P, Wigger T, Tong J, Marrow TJ. J-integral analysis: An EDXD and DIC comparative study for a fatigue crack. *Int J Fatigue* 2020;134:105474. <https://doi.org/10.1016/j.ijfatigue.2020.105474>.
- [17] Barhli SM, Mostafavi M, Cinar AF, Hollis D, Marrow TJ. J-Integral Calculation by Finite Element Processing of Measured Full-Field Surface Displacements. *Exp Mech* 2017;57:997–1009. <https://doi.org/10.1007/s11340-017-0275-1>.
- [18] Marrow J, Scotson D, Jin X, Chen H, Chen Y, Koko A, et al. Small-Specimen Testing, with Image-Based Analysis, for Crack Propagation Resistance in Polygranular Nuclear Graphite. *Graphite Testing for Nuclear Applications: The Validity and Extension of Test Methods for Material Exposed to Operating Reactor Environments*, ASTM International 100 Barr Harbor Drive, PO Box C700, West Conshohocken, PA 19428-2959; 2022, p. 1–17. <https://doi.org/10.1520/STP163920210051>.

- [19] Gontarz J, Podgórski J. Comparison of various criteria determining the direction of crack propagation using the udmgini user procedure implemented in abaqus. *Materials* 2021;14. <https://doi.org/10.3390/ma14123382>.